ELSEVIER

Nuclear Instruments and Methods in Physics Research A 459 (2001) 565–576

NUCLEAR INSTRUMENTS & METHODS IN PHYSICS RESEARCH Section A

www.elsevier.nl/locate/nima

Gamma-ray Compton camera imaging with a segmented HPGe

G.J. Schmid[a,*], D.A. Beckedahl[a], J.E. Kammeraad[a], J.J. Blair[b], K. Vetter[c], A. Kuhn[c]

[a]*Lawrence Livermore National Laboratory, L-231, Livermore, CA 94550, USA*
[b]*Bechtel Nevada, North Las Vegas, NV 89130, USA*
[c]*Lawrence Berkeley National Laboratory, Berkeley, CA 94720, USA*

Received 11 August 2000; accepted 29 August 2000

Abstract

In this paper, we investigate our concept to develop a γ-ray Compton camera out of a single coaxial High Purity Germanium (HPGe) detector. The imaging properties of the HPGe can be realized by way of a segmented outer contact and digital pulse-shape analysis. Limiting factors in performance will be related to the intrinsic electron momentum in Ge and the noise in the preamplifier JFETs. In addition to discussing these issues, we will present experimental and theoretical imaging studies that we have done using an existing segmented HPGe: the GRETA prototype detector at LBNL.

PACS: 29.40.G; 89.20. + a; 07.85

Keywords: Gamma-ray imaging; Segmented HPGe; Compton camera

1. Introduction

In the nuclear non-proliferation field, there is a need for portable γ-ray imagers that can quickly detect hidden or unseen quantities of highly enriched uranium (HEU). In order to achieve rapid identification, such imagers must have high absolute efficiencies at 186 keV (the γ-ray line of interest in ^{235}U). Furthermore, in order to achieve clear images via background rejection, high-energy resolution is also very important.

One approach to this problem is to use a large area position sensitive detector in concert with a coded aperture mask (a variant on pin-hole imaging). However, Compton camera imaging has certain advantages that are attractive over coded aperture imaging: it does not require a heavy metal collimator; it offers, potentially, a much larger field of view; and, furthermore, it is applicable to much higher γ-ray energies (several MeV) which may be of interest in a given scenario.

The standard Compton camera is a two detector coincidence system. Most commercially available Compton cameras use scintillators, but the energy resolution in these systems is not adequate for the current purpose. Du et al. [1] have recently described a Compton camera idea based on CZT crystals. However, even though CZT has a better

* Corresponding author. Tel.: + 1-925-423-7866; fax: + 1-925-422-3160.
E-mail address: gjschmid@llnl.gov (G.J. Schmid).

0168-9002/01/$ - see front matter
PII: S0168-9002(00)01028-7

energy resolution than most scintillators, its value is still below that of Ge.[1] In the Compton camera design of Phlips et al. [2], two planar Ge strip detectors (GSD) are used. However, despite the high-energy resolution, this type of system will suffer from low absolute efficiency due to the need to operate the two detectors in coincidence. Our novel idea for a Compton camera is to instead employ a single large volume, position sensitive, crystal of High-Purity Ge (HPGe), and to detect all those full energy events that Compton scatter within the detector. The position sensitivity of the crystal is realized by way of segmenting the outer contact, and performing digital pulse-shape analysis on all the signals for each event. The potential efficiency gain associated with this new design is estimated to be about 1 order of magnitude.

In what follows, we will discuss the details of our proposed approach, including advantages and limitations, and will present experimental and theoretical imaging studies that we have done using an existing segmented HPGe detector: the LBNL GRETA prototype.

2. Overview of HPGe imaging concept

We propose to develop a Compton camera imager using a 5 cm × 5 cm pure coaxial HPGe (hole diameter 1 cm). According to Monte Carlo simulations using the GEANT code [3], a 186 keV γ-ray that enters the front face of such a detector (from 20 cm away on axis) has a 70% chance of absorbing fully. Of those γ-rays that fully absorb, Monte Carlo simulations indicate that 43% will be single-site photoabsorptions, 32% will be 2-site events (Compton scatter + photoabsorption), and the remaining 25% will be events involving 3 or more sites (multiple Compton scatter + photoabsorption).[2]

For imaging, it is the 2-site events that are of primary interest. In particular, if one could experimentally determine the position and energy at both interaction sites, one could then use the energy-angle relationship of Compton scattering to determine θ_c, the Compton scattering angle. This angle then defines a cone of possible incident directions for the γ-ray, with the axis of the cone being in the direction $|\boldsymbol{X}_1 - \boldsymbol{X}_2|$ ($\boldsymbol{X}_1$ is the location of the Compton scattering site, and $\boldsymbol{X}_2$ is the location of the photoabsorption site), and θ_c being the half-angle. Over many events, these cones, if projected onto an image plane or image sphere, will overlap at the source position, thus giving an image.

For 2-site events at incident γ-ray energies greater than 256 keV, there is some ambiguity regarding which interaction site is associated with the Compton scatter, and which is associated with the photoabsorption. Fortunately, for incident γ-rays below 256 keV, kinematics dictates that the lower energy site is always the Compton scatter. This allows one to properly orient the direction of the cone axis in space.

Once one has selected out the 2-site events, an image can be formed. To maximize the image quality, one can impose the further constraint that the 2-site events must be separated by a distance that is large compared with the position resolution of the crystal. This will lower the efficiency of the imager, but will improve the angular resolution.

The position resolution of the HPGe crystal can be realized by way of a 36-fold segmented outer contact (the number of segments being limited to 40 or less by manufacturing concerns [4]). Each of the 36 electrically isolated contacts would have its own preamp and digitizer channel. For every γ-ray event in the crystal, we would seek to digitize the pulse-shapes on all 36 segments, and use this information to infer the number, location, and energy of all deposition sites in the crystal. This would be accomplished by assembling a set of calculated "basis functions" for single-site energy depositions throughout the crystal. Each basis function would consist of the response of all 36 segments to a unit energy deposition at a given location. By calculating a basis function for each point on a grid throughout the volume of the crystal, we can then take an arbitrary event (single or multiple-site) and

[1] For background rejection, the primary quantity of interest is the energy resolution of the total energy deposited (for an HPGe, should be ~1 keV for 186 keV γ-rays). The energy resolution of individual γ-ray interactions is also of interest, but, as will be discussed, is dominated by electron momentum effects.

[2] For the current discussion, a "site" is defined as a location of energy deposition in the crystal associated with a Compton scatter or photoabsorption interaction. The details of the electron tracks are ignored.

expand the measured signals in terms of the basis functions. The expansion coefficients are then the energy depositions at sites associated with given basis functions. In practice, this expansion could be performed by a χ^2 minimization procedure, whereby n combinations of basis functions are fit, in turn, to the measured pulseshape set (n being the number of interactions for the event).

As we will discuss in Section 5, this technique of determining the location of γ-ray interactions by pulse-shape analysis has already been experimentally demonstrated by us. Using the GRETA prototype detector at LBNL, we showed that it was possible to determine the location of single-site interactions at 374 keV to better than 1 mm (much smaller than the segment size). However, untangling multiple-site Compton events at 186 keV, and using this information to perform imaging, will be more complicated. In what follows, we address the feasibility of this concept.

3. Angular resolution

When a γ-ray Compton scatters off an atomic electron at rest, the energy-angle relationship is given by the following formula:

$$\cos\theta_c = 1 + \frac{511}{E_\gamma} - \frac{511}{E'_\gamma} \quad (1)$$

where θ_c is the Compton scattering angle, E_γ is the incident γ-ray energy (in keV), and E'_γ is the scattered γ-ray energy. The experimental determination of θ_c, given E_γ, E'_γ, and $|\boldsymbol{X}_1 - \boldsymbol{X}_2|$, is subject to certain errors that we now discuss.

3.1. Effects of energy uncertainty

Relationship (1) is derived by conservation of energy and momentum assuming the atomic electron is initially at rest. However, as discussed in Ref. [1], the atomic electron in Ge has a non-negligible intrinsic momentum, and thus Eq. (1) will be in error to an extent that depends on the exact value of the electron momentum at impact. Unfortunately, although the electron momentum distribution as a whole is well known [5], the exact value at impact is indeterminable (given that one knows only the deposited energies, and has no knowledge of the incident γ-ray direction). Therefore, the best that one can do is to continue to use Eq. (1), which is correct on average, but to realize that on an event-by-event basis, the measured energy deposition, $E_\gamma - E'_\gamma$, will vary from the average according to a particular probability distribution. This probability distribution is related to a convolution of the intrinsic energy resolution function of an HPGe (a Gaussian) with a kinematic function [6] dependent on E_γ, θ_c, and the electron momentum distribution. The value of E_γ, on the other hand, which is the total energy deposited (for a full absorption event), is not sensitive to electron momentum effects, and can be measured from the unsegmented inner contact of the HPGe (should be accurate to ~ 1 keV at 186 keV).

Fig. 1 shows graphically the effect of the electron momentum. For a Compton scattering event at 90°, 49.6 keV (on average) is deposited in the crystal. Without electron momentum effects, the energy resolution (fwhm) is ~ 1 keV. With electron momentum effects, one obtains a distribution which is very non-Gaussian, and has a 76% confidence level width (equivalent to a fwhm for Gaussian) of 9 keV. Using Eq. (1), this uncertainty in energy corresponds to an uncertainty in θ_c as shown in Fig. 2. The angular resolution is 15°. Fig. 3 shows how the angular resolution can be expected to vary with scattering angle.

3.2. Effects of position uncertainty

Due to noise in the measured pulseshapes, there will be an associated uncertainty in the deduced positions of the γ-ray interactions. While the energy uncertainties affect determination of θ_c, which is the half-angle of the probability cone, the position uncertainties will affect the determination of the cone axis direction. If one assumes that these uncertainties are dominated by uncertainties in the two transverse directions, and furthermore assumes that the uncertainties in these two directions are Gaussians with fwhm Δx, then the position-dependent angular resolution (fwhm), $\Delta\theta_p$, is

$$\Delta\theta_p = (2.35)\tan^{-1}\left(\frac{\Delta x\sqrt{2}}{(2.35)d}\right) \quad (2)$$

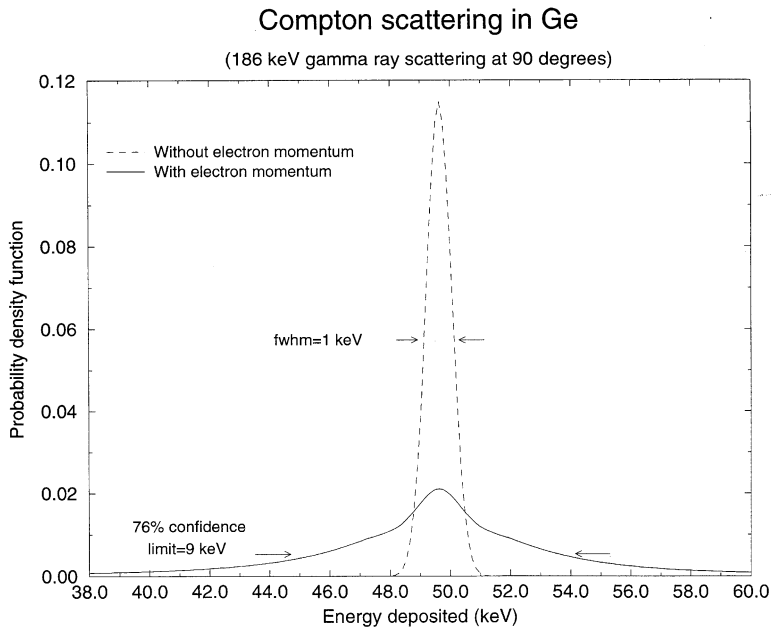

Fig. 1. Calculated energy deposition profiles ($E_\gamma - E'_\gamma$) with and without intrinsic electron momentum effects [5,6].

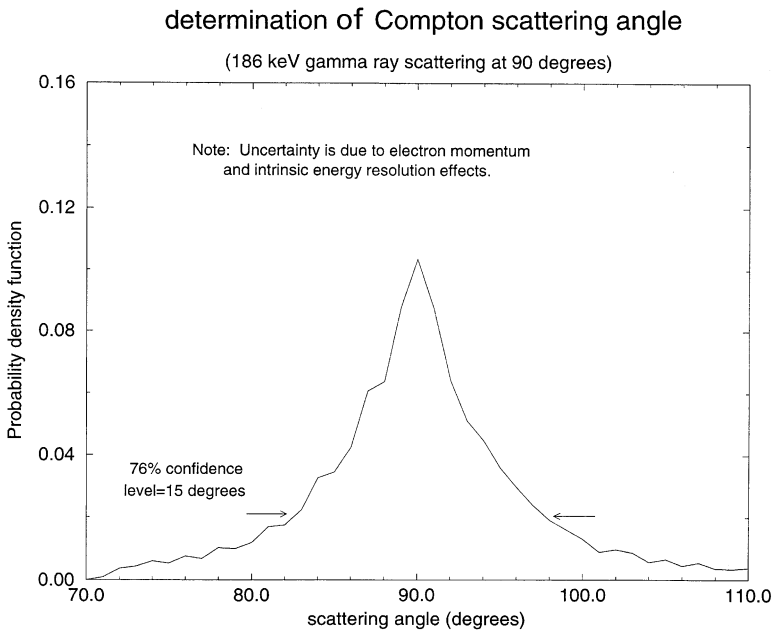

Fig. 2. Angular uncertainty in determination of Compton scattering angle. The histogram shown is generated by sampling the distribution in Fig. 1, and then converting to the angle coordinate.

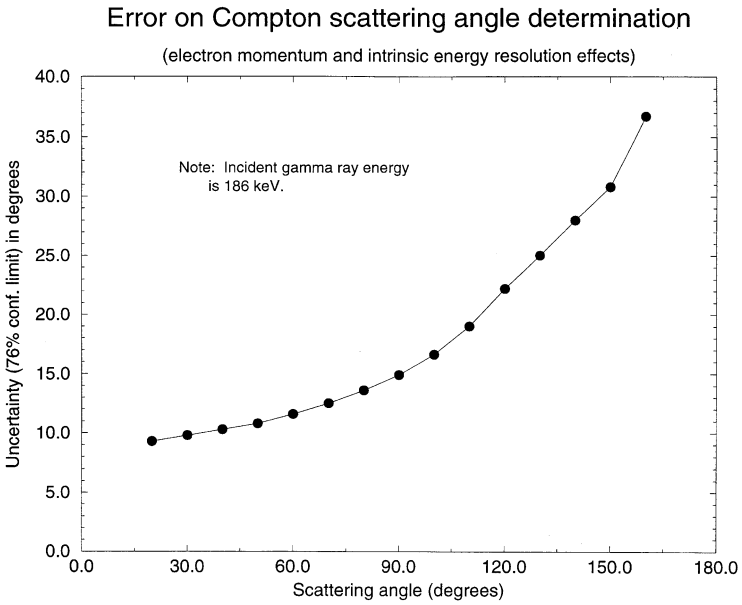

Fig. 3. Angular uncertainty versus true scattering angle. The uncertainties were obtained from angle distributions generated by sampling from the appropriate energy distribution (e.g. for 90° scattering, the distribution is Fig. 1).

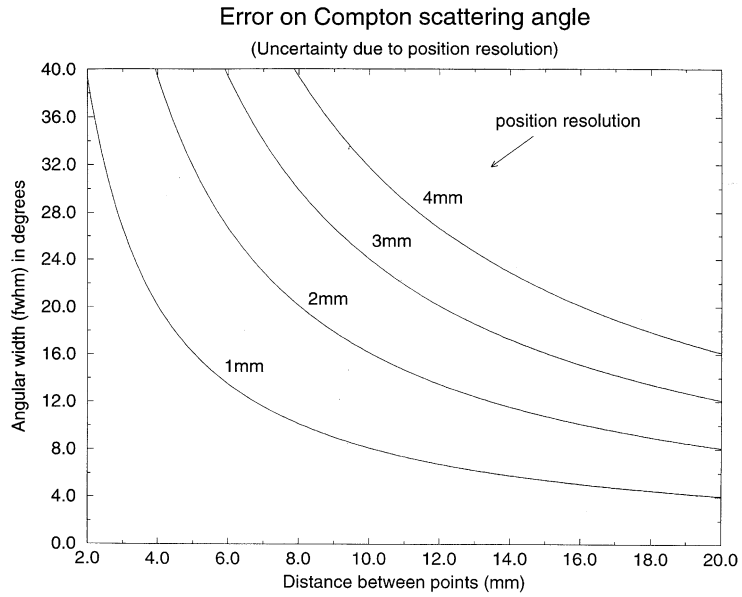

Fig. 4. Angular uncertainty in experimental determination of Compton scattering angle versus position resolution and distance between energy deposition sites.

where d is the distance between the interaction sites.

Fig. 4 shows $\Delta\theta_p$ as a function of d and Δx. To a good approximation, it should be independent of θ_c. As will be discussed in Section 6, $\Delta x \sim 1\,\text{mm}$ should be a reasonable estimate for the position resolution for our proposed imager. In this case, if one restricts acceptable events to those that have

$d \geq 8$ mm, the total angular resolution should be dominated by electron momentum effects in all cases (cf. Figs. 3 and 4).

4. Efficiency

4.1. Discarding unwanted events

In principle, the basis function expansion procedure outlined in Section 2 can yield the number, energy and position for all n interactions in a given γ-ray event. Any γ-ray event with two energy deposition sites, or more, could then be used to perform imaging (assuming full energy deposition). The events with more than two deposition sites could be analyzed using the methods of γ-ray tracking [7]. In particular, for a given event which has a given number of energy deposition sites, one can use Eq. (1) at each site to generate a most probable time-ordering of the points. In this manner, one can determine the first two scattering sites, and thus generate the probability cone for imaging.

However, looking for three or more energy deposition sites promises to be very time consuming in the basis function expansion procedure. To simplify matters, we propose to expand each measured pulse-shape set using only two basis functions (i.e. assume $n = 2$). Those events that are either single-site, or more than two sites, will not be well fit, and can thus be rejected at this stage. As explained in Section 2, this rejects about 68% of the events.

When one does Compton camera imaging, it is desirable that the performance of the camera be limited as much as possible by basic physics issues, and not by the physical characteristics of the camera. Therefore, we would hope to run our camera in a mode where the angular resolution is limited by the electron momentum issue, and not by the position resolution of the detector. As discussed in Section 3, this can be accomplished by requiring at least 8 mm between interaction sites. Unfortunately, throwing out events where $d < 8$ mm will reduce the 2-site efficiency by 73%.

Another cut that must be made is to throw out events where one of the energy depositions is not sufficiently high above the noise. As discussed in Section 5, a noise level per segment of $\sigma \sim 0.6$ keV seems feasible. If we require that all acceptable events must have energy deposition sites that are at least $5\times$ above the noise, we further reduce the efficiency by 8%.

One final issue to consider is that of elastic Rayleigh scattering. The fraction of Rayleigh to Compton scattering in Ge is $\sim 15\%$ at 186 keV [8], and even higher at lower energies. According to Monte Carlo simulation [3], 23% of otherwise acceptable events (as delineated above) will contain a Rayleigh scatter. Rayleigh scattering is a potential problem for Compton camera techniques because it can cause the probability cone axis to be misaligned. For example, if the γ-ray Rayleigh scatters before Compton scattering, the subsequent two energy depositions (e.g. Compton and photoelectric) will not define the correct cone axis. In fact, the correct cone axis is now the axis connecting the Rayleigh scattering vertex (zero energy deposition) with the Compton scatter vertex. The axis-shifting effect of Rayleigh scattering, when it occurs, can be substantial (tens of degrees). Fortunately, it occurs seldom enough so that it is not of primary concern.

4.2. Overall performance compared with "standard" Compton Camera design

It is of interest to compare the performance of proposed imager with that of a "standard" Ge coincidence system. For comparison purposes, we choose a variation on the Compton camera design presented in Ref. [2]. Using Monte Carlo simulation, we have modeled the detector geometry of Phlips et al. [2] using the Fig. 1 in that paper. However, the centers of the two Ge strip detectors are placed much closer, 5 cm apart in the source direction, to maximize efficiency. The two Ge detectors are assumed to have adequate position resolution so that the angular resolution is dominated by electron momentum effects. This would require a higher position resolution than presented in Ref. [2], but is assumed to be possible.

The angular resolution for this comparison case should be similar to our own due to the fact that both designs are dominated by electron momentum effects. The primary difference will be efficiency. According to simulation, the comparison case should have an absolute efficiency of 1.3×10^{-5} for

a 186 keV γ-ray source placed 20 cm in front of the vertical detector. This efficiency counts only "good" events: full energy events that have a single deposition site in each detector. The corresponding absolute efficiency for our current design is 2.1×10^{-4}. This number counts only full absorption, 2-site, events that are separated by at least 8 mm, and have energy depositions at least $5\times$ above the expected noise of 0.7 keV. This "imaging" efficiency of 2.1×10^{-4} is about a factor of 12 below the full photopeak efficiency for a 5 cm × 5 cm HPGe.

The comparison discussed above reveals that a gain of $\times 16$ in efficiency may be possible for the current design. If one normalizes this efficiency gain to the volume of Ge employed ($\times 1.88$ greater for the current design), one still realizes about a factor of 9 efficiency gain.

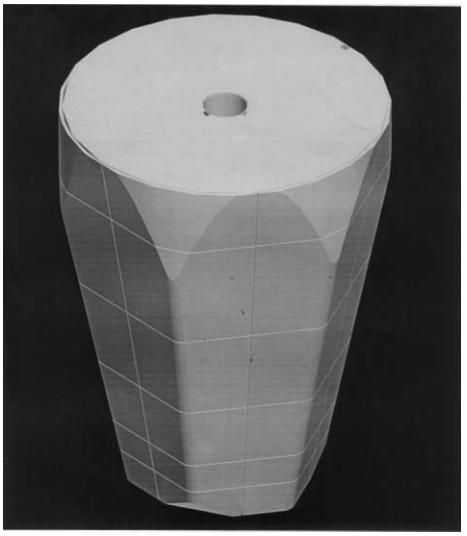

Fig. 5. Geometry of GRETA prototype detector as represented by computer simulation code MAXWELL 3-D [10].

5. GRETA prototype imaging tests

In theory, the HPGe imaging concept seems viable, but what about in practice? This question was partially addressed in Ref. [9], where we performed imaging simulations involving an HEU detection scenario. The detector was assumed to be a 5 cm × 5 cm pure coax with 1 mm spatial resolution (the electron momentum effects were also included in the simulation). The imaging results seemed acceptable given the expected limitations.

In order to compliment the computer simulations of Schmid et al. [9], experimental results are also desired. This was accomplished recently by undertaking a series of measurements using an existing segmented HPGe detector: the GRETA prototype detector at LBNL. This detector, a coaxial, tapered hexagon in shape, has 36 segments on the outer contact, each segment having its own preamp (10–90% risetime of ~ 25 ns) and its own digitizer channel (500 million samples per second). While some aspects of this detector are not ideal for our purposes, most notably the unconventional geometry (the detector was designed for accelerator-based nuclear physics studies, not low-energy γ-ray imaging), it is nevertheless an interesting test case. Fig. 5 shows a computer model of the GRETA detector that was designed using the software code MAXWELL 3-D [10]. The segmentation scheme is visible on the outside surface of the detector. The total length of the detector is 9 cm, the front face is 4.4 cm at its widest point, and the back face is circular and 7 cm wide. The segments are labeled A–F azimuthally (clockwise around the detector symmetry axis), and 1–6 in depth (moving from front face to back face). For example, the 4th segment up from the beveled edge of the front face is labeled segment B4. Segments A4 and C4 are then right and left azimuthally.

5.1. Pulse-shape calculations

Theoretical basis functions (i.e. calculated pulse-shape sets for unit energy depositions at given locations) were determined on a 2 mm Cartesian grid throughout volume. Details of the theoretical calculations follow the procedure outlined in Ref. [11], with the exception that a more rigorously correct geometry was employed this time (as shown by Fig. 5). The MAXWELL 3-D finite element code was used to solve for the total electric field assuming $+3000$ V on the inner contact, 0 V on the outer contact, and a charge impurity density as specified in Ref. [11]. The same code was also used to calculate the segment weighting fields by assuming $+1$ V on segment of interest, and zero volts on

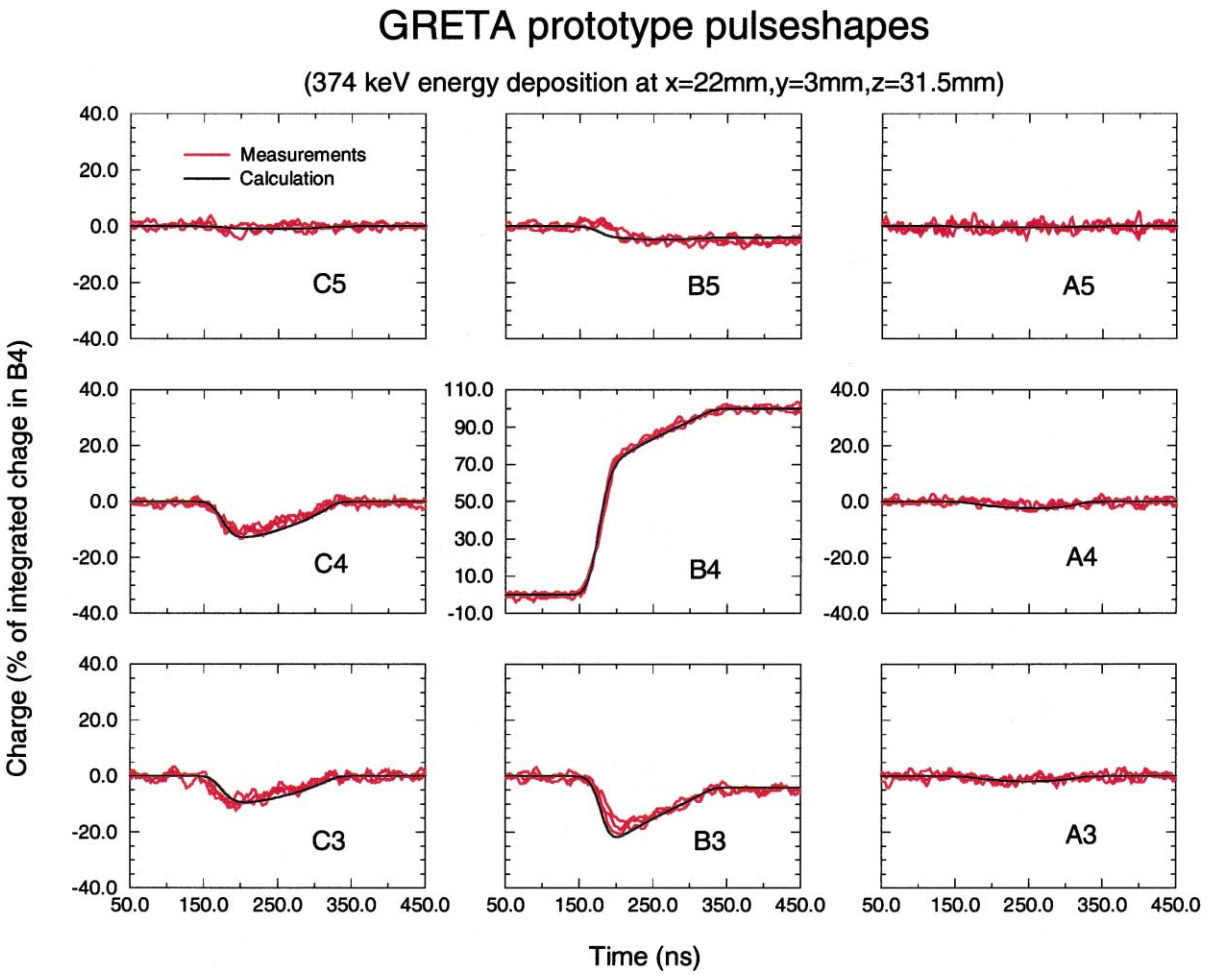

Fig. 6. GRETA pulseshapes for 374 keV energy deposition at the given location inside segment B4 (the x–y–z coordinate system is the same as in Fig. 7). A 4% cross-talk between the B segments has been corrected for in this picture.

every other segment. This information, along with known electron/hole mobilities, can then be used to calculate pulseshapes for given locations inside the crystal.

Fig. 6 shows, by the smooth solid lines, a calculated pulse-shape set for energy deposition at a given point inside segment B4. This set includes the signal on the primary contact, B4, as well as the signals on the eight surrounding contacts. In addition to the calculated pulseshapes, 3 measured pulse-shape sets are shown superimposed (the traces with fluctuating noise). These measurements were acquired as part of a recent experimental program [11] to use a collimated radioactive source to probe the GRETA crystal with specified energy depositions at specified locations. In particular, 662 keV γ-rays from a ^{137}Cs source were scattered at 90° in the crystal so as to allow measurements of pulse-shape sets for a 374 keV energy deposition. By detecting the scattered 288 keV radiation in a second detector, background events could be minimized. The agreement between calculation and experiment is seen to be quite good. In principle, the signal on the primary

contact gives information about the radial coordinate of the energy deposition, while the signals on the neighboring contacts give information about the azimuthal and depth coordinates.

A mathematical analysis of these results [11], which concerned the spatial variation of the average pulseshape as compared with the noise, demonstrated that 0.5 mm fwhm "position sensitivity" was obtainable at 374 keV throughout the spatial region studied. If we take this position sensitivity to be an estimate of the event-by-event position resolution at 374 keV, we can then determine values for the position resolution at other energies. For example, since the signal-to-noise, and hence the position resolution, varies linearly with energy, we can expect a position resolution of 3.7 mm at 50 keV.

5.2. Experimental imaging test at 244 keV

Using a ^{152}Eu source, we took some data with the GRETA prototype to see if imaging was possible. The 244 keV γ-ray line in a ^{152}Eu source was used to mimic a 186 keV line from HEU. Fig. 7 shows the geometry of the experiment, the source being placed 15 cm away from segment B4. The origin of coordinate system shown is at the center of front face, with the z-axis pointing through the crystal along symmetry axis, and the y-axis pointing towards a beveled edge. Each measured pulseshape set (corresponding to the interaction and absorption of one γ-ray) was expanded into 2-combination sets of calculated basis functions as discussed earlier (in this case, basis functions include the effects of the preamp responses). The basis functions covered Cartesian space in 2 mm steps, and energy space in 10 keV steps. An algorithm was also added so as to allow interpolation between basis functions. Cuts in the data were made so as to discriminate against non-2site events (by accepting only good fits), noisy events (events with 1 site too close to noise level), and also large angular error events (by defining an acceptable angular scattering range).

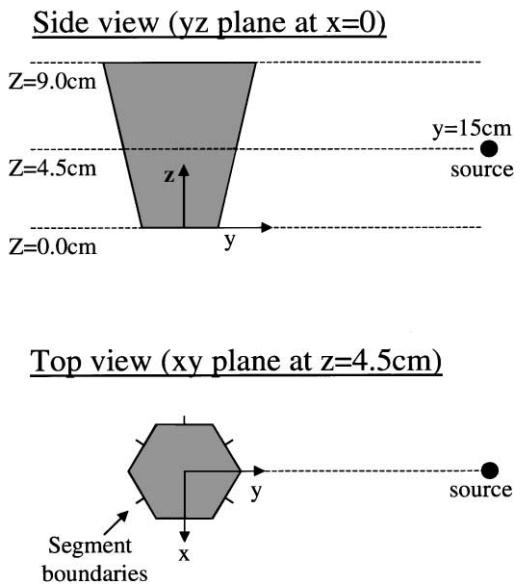

Fig. 7. Geometry for experimental GRETA imaging test. The source is ^{152}Eu.

The top image in Fig. 8 shows the results. These images represent the world, in spherical coordinates, as seen from the center of the HPGe. The azimuthal ϕ coordinate is weighted by $\sin\theta$ so as to give equal area to each square pixel in the image. As can be seen from the figure, the source is not correctly located (only a false "ghost image" due to noise is seen). The source was then rotated around the detector symmetry axis by 90° to produce the image in the bottom of Fig. 8. Again, no sensible image was produced.

5.3. Imaging simulation at 186 keV

To address the question of why the imaging experiment failed, a Monte Carlo based imaging test was performed using the same geometry as Fig. 7. The Monte Carlo code GEANT [3], modified to allow for inclusion of intrinsic electron momentum effects, was used to generate interaction points in the GRETA crystal. Pulse-shape sets were then generated for each event.[3] To create

[3] A given event could consist of a single-site photoabsorption, a multiple-site deposition, or even a Compton escape. The effects of Rayleigh scattering are included. In the imaging analysis that follows, the knowledge of what actually happened is not used: as in real-life, one has only the pulse shapes.

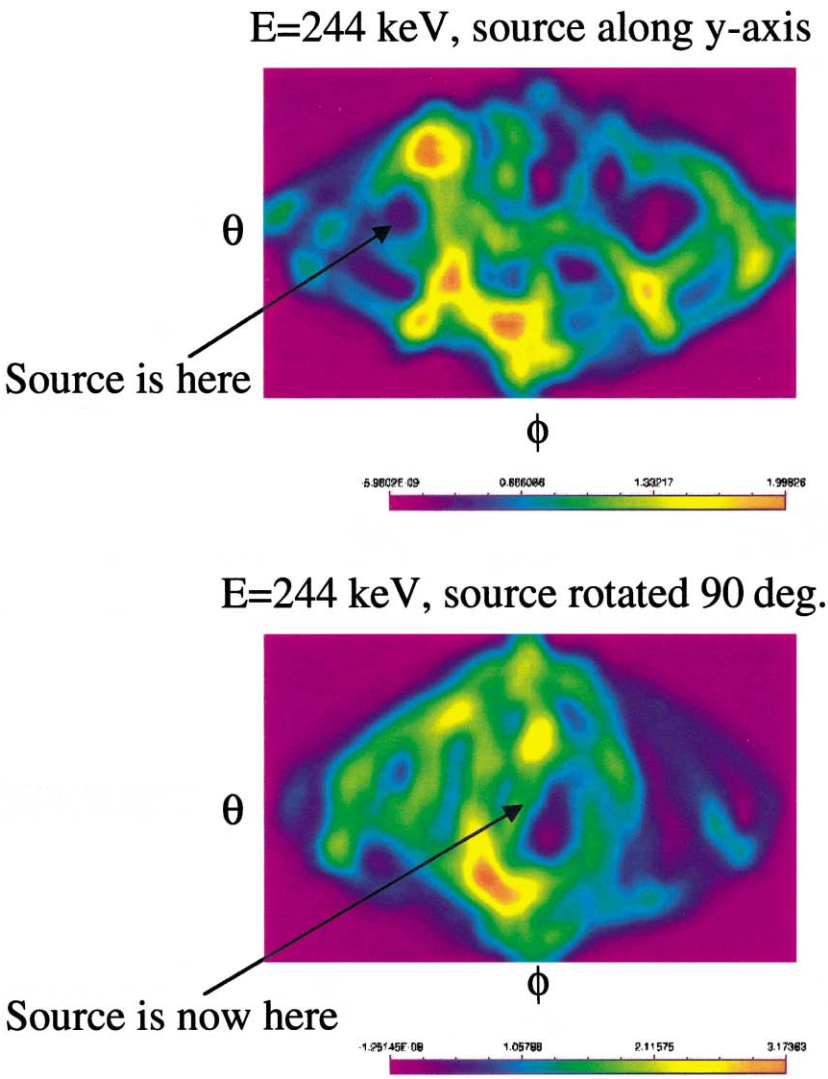

Fig. 8. Results of experimental GRETA imaging tests at 244 keV. Top: original source geometry; Bottom: source rotated $+90^{\circ}$ about z-axis. The total number of gamma ray events, before downselecting, is 792 and 238, respectively.

the artificial data, real (measured) noise was added to the calculated signals ($\sigma = 4$ keV). The known preamp response functions were convolved in as well. This artificial data was then run through the same basis function expansion and data cut procedure as before (with one difference: the 10 keV energy steps in the basis function fitting were changed to 5 keV energy steps). The resulting image is shown in the top of Fig. 9. Only a false ghost image is seen.

The most likely culprits for the image failure are the signal noise (preamp JFET noise) and the electron momentum problem. Since there is nothing that can be done to address the later issue, we focused on the former. For an ideal HPGe γ-ray imager, what are the best noise properties that can be realized? In principle, the real quantity of interest for determining the noise level in keV is the signal-to-noise ratio, V_s/V_n, where V_s is the signal voltage at the preamp output, and V_n is the JFET

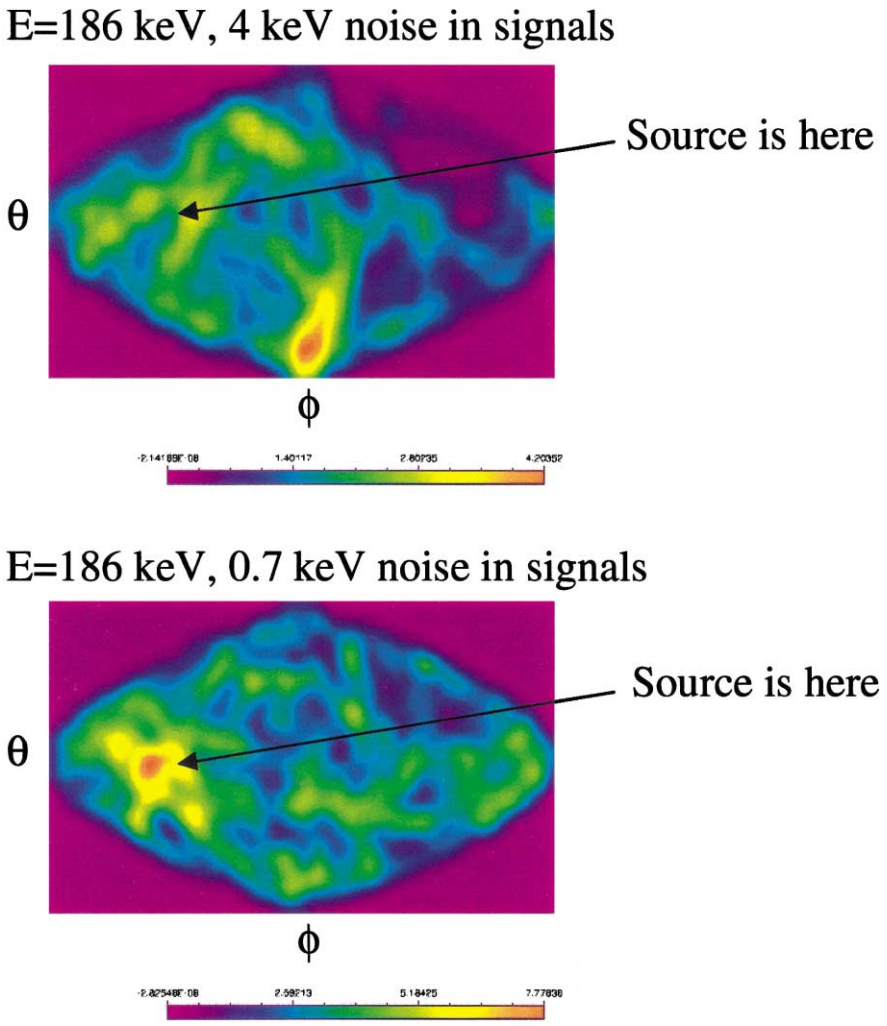

Fig. 9. Results of simulated GRETA imaging tests at 186 keV (same geometry as Fig. 7). Top: pulseshape noise is 4 keV rms, and only a false ghost image is seen; Bottom: pulseshape noise is 0.57 keV rms, and the source is now correctly located. The total number of gamma ray events, before downselecting, is 408 and 356, respectively.

noise voltage at the same location. This ratio can be given by

$$\frac{V_s}{V_n} = \frac{Q}{Cv_n} \tag{3}$$

where Q is the total charge deposited by the γ-ray, C is the total capacitance seen by the segment of interest, and v_n is the JFET input noise voltage [12]. The total capacitance, C, should (for low values of the preamp feedback capacitor) be approximately equal to the sum of the following capacitances: the capacitance of the segment to the inner contact; the capacitance of the segment to the grounded Al can surrounding the crystal; and the capacitance of the segment to ground through the JFET in the preamp. For the GRETA prototype, these 3 contributions are estimated (for a segment in the middle) to be: 1.6, 7, and 15 pF, respectively. The large contribution of the Al can be due to its

close proximity to the crystal (1 mm distance).[4] For the JFETs in the GRETA preamps, v_n is given as $15\,\mathrm{nV}/\sqrt{\mathrm{Hz}}$.

For an ideal coaxial HPGe imager, we can improve upon these numbers. First of all, the grounded Al can could be moved much further back, thus reducing the total segment capacitance by 7 pf. Furthermore, instead of the current JFET's, we would use the Pentafets described in Ref. [13] (design PF2). These JFETs have capacitances of 1 pF and noise voltages of $2\,\mathrm{nV}/\sqrt{\mathrm{Hz}}$. Incorporating these two changes would reduce the Cv_n product by a factor of 7, thus increasing the signal-to-noise ratio by a factor of seven, and reducing the measured noise level from $\sigma = 4\,\mathrm{keV}$ to $\sigma = 0.57\,\mathrm{keV}$. This reduced noise level would allow the 50 keV position resolution to be lowered from 3.7 to 0.5 mm.

Using this new noise level, the Monte Carlo based imaging test described above was repeated. The result is on the bottom of Fig. 9. This time, the image appears exactly where it is expected (within error) at $\phi = 90^\circ$, $\theta = 90^\circ$. This would appear to demonstrate that HPGe γ-ray imaging is indeed possible if noise levels can be substantially reduced (and if pulse-shape sets can be calculated to the required accuracy).

6. Conclusion

We have discussed here our idea for developing a γ-ray Compton camera out of a single HPGe detector with a segmented outer contact. In pursuit of this goal, we have undertaken a testing program utilizing the GRETA prototype at LBNL, an existing 36-fold segmented HPGe. Our results indicate that the GRETA prototype is not ideal for 186 keV γ-ray imaging due to its high noise levels. However, we have argued that noise levels could be reduced by changing the geometry of the Al shielding can, and by changing the JFETs used in the preamps. If noise levels a factor of seven below the GRETA prototype can be achieved, γ-ray imaging then seems possible (with limitations as discussed here-in).

[4] The Al can was purposely set this close so as to simulate the environment of a close-packed array of detectors (useful for accelerator-based nuclear physics applications). For our current γ-ray imaging application, the Al can would be better if moved much farther away.

Acknowledgements

One of the authors (GJS) would like to thank K.P. Ziock for helpful discussions. This work has been performed at the UC LLNL and LBNL under the auspices of the US DOE under contract W-7405-Eng-48.

References

[1] Y.F. Du, Z. He, G.F. Knoll et al., Proc. SPIE 3768 (1999) 228.
[2] B.F. Phlips, S.E. Inderhees, R.A. Kroeger et al., IEEE Trans. Nucl. Sci NS-43 (1996) 1472.
[3] R. Brun, F. Bruyant, M. Maire et al., GEANT 3.21 Monte arlo package, CERN, Switzerland, 1987.
[4] K. Knight, private communication.
[5] F. Biggs, L.B. Mendelsohn, J.B. Mann, Atom. Data Nucl. Data Tables 16 (1975) 201.
[6] D. Brusa, G. Stutz, J.A. Riveros et al., Nucl. Instr. Meth. A 379 (1996) 167.
[7] G.J. Schmid, I.Y. Lee, M.A. Deleplanque et al., Nucl. Instr. Meth. A 430 (1999) 69.
[8] E. Storm, H.I. Israel, Nucl. Data Tables A 7 (1970) 565.
[9] G.J. Schmid et al., in the Proceedings of the 41st annual meeting of the Institute of Nuclear Materials Management (INMM), New Orleans, LA, July 16–20, 2000.
[10] MAXWELL 3-D Field Simulator, Ansoft Corp., Pittsburgh, PA, 1999.
[11] K. Vetter et al., Nucl. Instr. Meth. A 452 (2000) 223.
[12] J. Blair, D. Beckedahl, J. Kammeraad, G. Schmid, Nucl. Instr. Meth. A 422 (1999) 331.
[13] T. Nashashibi, Nucl. Instr. Meth. A 322 (1992) 551.